ACS APPLIED MATERIALS & INTERFACES

RESEARCH ARTICLE

www.acsami.org

PEMFC Catalyst Layers: The Role of Micropores and Mesopores on Water Sorption and Fuel Cell Activity

Tatyana Soboleva,[†,‡] Kourosh Malek,[‡] Zhong Xie,[‡] Titichai Navessin,[‡] and Steven Holdcroft[†,‡,*]

[†]Department of Chemistry, Simon Fraser University, 8888 University Drive, Burnaby, British Columbia, Canada V5A 1S6

[‡]Institute for Fuel Cell Innovation, National Research Council Canada, 4250 Wesbrook Mall Vancouver, British Columbia, Canada V6T 1W5

ABSTRACT: The effects of carbon microstructure and ionomer loading on water vapor sorption and retention in catalyst layers (CLs) of PEM fuel cells are investigated using dynamic vapor sorption. Catalyst layers based on Ketjen Black and Vulcan XC-72 carbon blacks, which possess distinctly different surface areas, pore volumes, and microporosities, are studied. It is found that pores <20 nm diameter facilitate water uptake by capillary condensation in the intermediate range of relative humidities. A broad pore size distribution (PSD) is found to enhance water retention in Ketjen Black-based CLs whereas the narrower mesoporous PSD of Vulcan CLs is shown to have an enhanced water repelling action. Water vapor sorption and retention properties of CLs are correlated to electrochemical properties and fuel cell performance. Water sorption enhances electrochemical properties such as the electrochemically active surface area (ESA), double layer capacitance and proton conductivity, particularly when the ionomer content is very low. The hydrophilic properties of a CL on the anode and the cathode are adjusted by choosing the PSD of carbon and the ionomer content. It is shown that a reduction of ionomer content on either cathode or anode of an MEA does not necessarily have a significant detrimental effect on the MEA performance compared to the standard 30 wt % ionomer MEA. Under operation in air and high relative humidity, a cathode with a narrow pore size distribution and low ionomer content is shown to be beneficial due to its low water retention properties. In dry operating conditions, adequate ionomer content on the cathode is crucial, whereas it can be reduced on the anode without a significant impact on fuel cell performance.

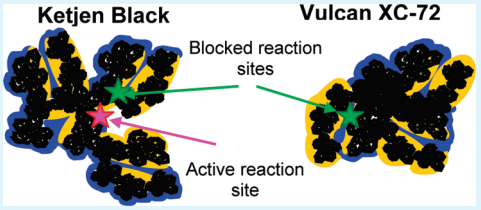

KEYWORDS: PEM fuel cell, catalyst layer, microstructure, water sorption, water retention, Ketjen Black, Vulcan XC-72

INTRODUCTION

Major advancements in catalyst layer (CL) development for PEM fuel cells were achieved upon replacement of Pt black with Pt supported on high surface area carbon, and impregnation of the CL with a PFSA ionomer.[1] Additional improvements were realized by introducing PFSA ionomer directly into the catalyst ink, through extension of the reaction zone and increased catalyst utilization.[2] Detailed reviews of these advancements can be found in the literature.[3] Conventional catalyst layers of PEM fuel cells comprised Pt catalyst supported on carbon black and the Nafion ionomer.[4] The rates of the electrochemical reactions in the CL depend on the surface area of Pt that is in contact with the reactant gas and the proton-conducting phase. A high surface of carbon support is necessary for the effective distribution of Pt nanoparticles, whereas the porosity of the support appears crucial for the incorporation of ionomer and for providing gas access to the reaction sites. It is widely recognized that the ionomer content in the catalyst layer has a great impact on gas transport properties - the higher the ionomer loading, the lower the available pore space for gas transport.[5] An optimum value of ~30 wt % ionomer is often adopted, which is believed to provide a sufficient ionomer network for proton conduction while leaving sufficient pore space for adequate gas transport. The ionomer distribution greatly depends on the pore size distribution (PSD), surface area and the nature of the carbon support employed.[6]

Typical carbon supports, such as Ketjen Black and Vulcan XC-72, are considered to be high surface area materials, having surface areas of ~900 and 220 m^2/g, respectively. The very high surface area of Ketjen Black is due to micropores, i.e., pores <2 nm diameter, within the carbon particle. These pores constitute >50% of the total surface area of Ketjen Black carbon.[6] However, it is suggested that the necks of micropores serve as nucleation sites for Pt particle deposition, thus rendering a large fraction of the internal microporous surface area unavailable for Pt distribution and inaccessible for fuel cell reactions. Moreover, it was found, and also predicted by modeling studies,[7] that the ionomer is distributed on the surface of agglomerates of carbon particles, i.e., in mesopores >20 nm diameter.[6] This has several implications for the design of catalyst layers. First, only the surface area of pores larger than ~20 nm is available for distributing the ionomer; hence, an increase in carbon surface area through introduction of microporosity, as in Ketjen Black, might not result in the efficient distribution of ionomer. An optimal quantity of ionomer in the CL is highly specific to the mesoporous surface area of the carbon and thus 30 wt % ionomer cannot be optimal for carbons that differ in mesoporous surface area.

Received: November 7, 2010
Accepted: May 16, 2011
Published: May 16, 2011

Second, Pt particles deposited in the pores <20 nm inside agglomerates are not necessarily in direct contact with ionomer and thus their participation in fuel cell reactions is debatable. In the agglomerate model refined by Eikerling et al,[7a] ionomer is assumed to be distributed on the surface of agglomerates, and intra-agglomerate space is filled with water. Water is believed to provide the path for proton conduction to and from Pt particles that are not in direct contact with ionomer. However, very little is known about where and how water is sorbed, distributed, retained or desorbed from the catalyst layer. The majority of published work to date on the topic is related to water transport in the proton exchange membrane (PEM),[8] gas diffusion layer (GLD),[9] and flow fields.[10] Information on the role of the CL on fuel cell water retention and transport is scarce despite the fact that the cathode catalyst layer is believed to be a key component in regulating the balance between water fluxes in an MEA.[7a]

In this work, we investigate water sorption and retention properties of CLs based on Ketjen Black and Vulcan XC-72 carbons as a function of ionomer content and relative humidity and correlate the data to catalyst layer microstructure. Electrochemical properties and fuel cell performances are correlated to water contents and microstructural properties of the CLs. Finally, the fuel cell performance of MEAs with distinctly hydrophilic properties of the anode and the cathode catalyst layer are examined.

EXPERIMENTAL SECTION

Materials. Ketjen Black carbon and Vulcan XC-72 carbon were received from Tanaka Kikinzoku Kogyo (TKK) and Cabot Corp., respectively. Catalyst powders with 46 wt % Pt on Ketjen Black (TEC10E50E) and Vulcan XC-72 (TEC10V50E) were received from Tanaka Kikinzoku Kogyo. Catalyst inks for spray deposition were prepared by mixing catalyst powder, Pt/carbon (Pt/C), in water and methanol mixture (1:1), corresponding to 0.70 g Pt/C in 100 g of water/methanol solution. The dispersion was sonicated for 30 min, while adding dropwise 0.74, 6.0, and 14 g of 5 wt % Nafion solution (Alfa Aesar) to the mixture to produce 5, 30, and 50 wt % ionomer loadings, respectively. The final mixture was sonicated at room temperature for 2 h.

All CLs comprising of Pt, carbon and ionomer were fabricated by spray-deposition on Nafion 211 membrane, which was used as received, producing CCMs with identical CLs on the cathode and the anode side for symmetrical CCMs. Two asymmetrical CCM types comprised of Vulcan 5 wt % anode and Ketjen Black 30 wt % cathode and vice versa. Spray deposition of the ink on Nafion 211 membrane was performed at 80 °C. CLs with 5, 30, and 50 wt % of ionomer were prepared corresponding to 0.1, 0.8, and 1.8 ionomer to carbon dry weight ratios (I/C ratios). Carbon and Pt loadings in all CLs were held constant at 0.475 mg/cm^2 and 0.4 mg/cm^2, respectively.

Methods. A DVS Advantage chamber from Surface Measurement Systems (SMS) was used to perform water vapor sorption experiments. Water uptake of samples was evaluated at 25 °C in the range of relative humidity from 0 − 97% RH with 10% RH steps from 0 to 90% RH, then to 95 and finally 97% RH. Desorption isotherms were recorded following a backward sequence of RHs. CCM samples were suspended on a wire so that the film freestanding conditions were maintained. Samples were equilibrated at each RH stage using a dm/dt parameter of 0.0002%/min (change in mass (dm) over time (dt)). N_2 gas, 99.95%, was used as a carrier gas and deionized water was used to humidify the carrier gas. A Nafion 211 isotherm was used as a blank to separate contributions of the membrane and the CLs to the total amount of water vapor sorbed by a CCM. Water uptake in a CL was found by subtracting the water content in Nafion 211 membrane from the total water uptake by a sample of a CCM. Water uptake of the CLs is expressed as the mass of water at each RH normalized to carbon content in the sample. The carbon content in CLs was calculated from the known Pt loading and the known ratio of Pt to carbon in Pt/C powders.

Cyclic Voltammetry (CV). Cyclic voltammetry was used to estimate electrochemically active surface area (ESA) and double layer capacitance (C_{DL}) of the CLs in the 20 − 100% RH range. Prior to CV measurements, the cell was conditioned using evaporation−condensation cycles: the cell was heated to 80 °C at 100% RH while H_2 was fed to the anode and N_2 to the cathode for 1 h, then cooled to ∼30 °C, while gases were kept at 80 °C to allow sufficient water condensation in the CL. The cell was then heated to 80 °C and the CVs were recorded. The cycle was repeated until no change in the CV shape was observed (3−5 cycles). H_2 adsorption and desorption currents on Pt were measured while H_2 was fed to the anode and N_2 to the cathode at 1 atm (abs). A Solatron 1287 potentiostat was used, the potential was scanned between 0.04 and 1.1 V vs SHE at a scan rate of 50 mV/s in the range of 100 − 20% RH in the downward scan with 10% RH steps. Gas flow rates of 0.2 L/min on the anode and no gas flow on the cathode were used. ESA was calculated from charges corresponding to Pt−H adsorption in the range from 0.08 to 0.45 V using Corrware software accounting for double layer charging and H_2−crossover currents. Double layer capacitance (C_{DL}) was calculated from the double layer charging current in the range 0.4 − 0.6 V subtracting H_2−crossover current. H_2−crossover current was measured using chronoamperometry in the 0.2 − 0.5 V range with a step of 0.1 V. Each potential step was held for 3 min in order to minimize the contribution from the charging current. The value of the current at the end of each potential step was plotted versus corresponding potential. The H_2-crossover current was estimated from the intercept of the plot with the ordinate.

Electrochemical Impedance Spectroscopy (EIS). The proton conductivity of CLs was evaluated using EIS while H_2 was fed to the anode and N_2 to the cathode. EIS was employed at 0.45 V imposing a 10 mV amplitude sinusoidal (AC) signal and a frequency range 15 kHz to 0.01 Hz using a Solatron 1287 potentiostat and a 1260 frequency analyzer. Impedance spectra were recorded under 100−20% RH in 10% RH steps. Proton resistance of CLs was estimated from Nyquist plots that had two characteristic slopes: the first slope at ∼45° angle in the high frequency region due to proton resistance in the CL, the second slope at an angle between 55 and 90° at lower frequencies dominated by the capacitance of the CL. By extrapolating the second slope to the Z'-axis, the proton resistance of the cathode CL was found as a difference between the extrapolated linear intercept and the intercept of the Nyquist plot with the Z'-axis (membrane resistance), multiplied by 3:[11]

$$R_p = 3(Z'_{LF} - Z'_{HF}) \quad (1)$$

where R_p is proton resistance, Z'_{LF} is the low frequency intercept, and Z'_{HF} is the high-frequency intercept of the Nyquist plot.

In the low RH condition and in CLs with very low ionomer loading, the transition between slopes was poorly defined. Thus, the proton resistance was estimated from the linear slope of the EIS spectrum in the range 1×10^4 to 1×10^3 Hz, which represents contributions from proton resistance and double layer charging capacitance of the CL and is expressed as follows:[12]

$$Z = \sqrt{\frac{R_p}{C_{dl}}}\omega^{-1/2} \quad (2)$$

where Z is the magnitude of the real part of impedance, R_p is the proton resistance, C_{DL} is the double layer capacitance, and ω is the frequency (equal to $2\pi f$). By plotting Z vs $\omega^{-1/2}$, the slope $(R_p/C_{dl})^{1/2}$ can be found. Double layer capacitance value determined from CV at each given

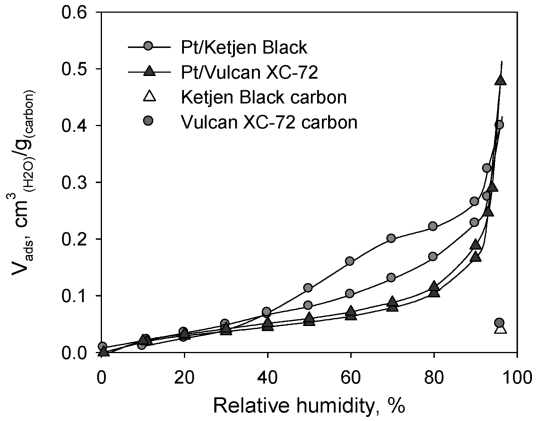

Figure 1. Water vapor sorption isotherms of Pt/Ketjen Black (triangles) and Pt/Vulcan XC-72 (circles) catalyst powders. The sorption capacity of Ketjen Black and Vulcan XC-72 carbon powders are shown at 97% RH.

RH at ~0.45 V was used to estimate the resistance to proton conduction in the CL.

EIS experiments performed with H_2 fed to the anode and O_2 to the cathode under increasing operational current densities were used to quantify the uncompensated resistance of the cell, R_U, (i.e., membrane, cell and cell hardware resistances), under 20 and 100% RH. H_2/O_2 EIS was recorded in the frequency range 20 kHz to 0.1 Hz and increasing current densities (0.04 A/cm^2 to ~1 A/cm^2). R_U was determined from the high frequency intercept of the Nyquist plot with the Z'-axis.

Polarization Performance. MEAs were assembled in a 25 cm^2 single cell with triple serpentine flow channels from Fuel Cell Technologies Inc. Polarization curves were recorded on a 850C test station from Scribner Associates Inc. Prior to obtaining IV polarization data, the cell was conditioned at 80 °C and 100% RH in the potential range between 0.9 and 0.6 V in 0.05 V steps.

Polarization data were collected by scanning the cell voltage from open circuit voltage (OCV) to 0.2 V in 0.05 V steps (120 s at each potential point). The cell temperature was 80 °C at atmospheric pressure. IV curves were recorded under dry (20% RH) and fully humidified conditions (100% RH). Scans were repeated five times to ensure reproducibility within each MEA.

RESULTS AND DISCUSSION

Water Vapor Sorption in Carbon and Pt/C Catalyst Powders. Water vapor sorption isotherms of Pt/Ketjen Black and Pt/Vulcan XC-72 normalized to carbon mass are shown in Figure 1. Vapor sorption capacity of carbon powders is found to be extremely low, e.g., ~ 0.03 cm$^3/g_{(carbon)}$ at 97% RH for both Ketjen Black and Vulcan XC-72 carbons (two data points at 97% RH). A low sorption capacity of carbon powders is indicative of their hydrophobic nature. Contact angles for Ketjen Black and Vulcan XC-72 carbons are reported to be 84° and 79°, respectively.[13] However, when Pt is deposited on carbon, the Pt/carbon powder is considerably more hydrophilic due to the wetting properties of Pt,[14] as shown in Figure 1 and illustrated by the isotherms.

Both Pt/carbon isotherms are Type 3 in nature with little sorption at low RH and an exponentially increasing sorption in the higher RH range.[15] This type of adsorption isotherm is characteristic of strong intermolecular gas interactions and a weak gas-adsorbent interaction. The former is typical of water vapor due to the propensity of water molecules to form hydrogen bonds. The latter is due to weak interaction between polar water molecules and the relatively nonpolar carbon black.[16] Sorption below 30% RH is comparatively low, as typical for Type 3 adsorption isotherms, due to adsorption of adsorbate molecules on the polar sites, as opposed to formation of a monolayer as in the case of a nonpolar adsorbent such as nitrogen.[17] Hence, it is assumed that in the low RH condition, water molecules adsorb first on the hydrophilic sites, such as Pt particles, oxygen containing functional groups on carbon, and edge sites of carbon crystallites.[18] In the intermediate range of RH, water molecules form multilayers around hydrophilic sites due to hydrogen bonding and, when these localized clusters of water are large enough, they coalesce; concurrently capillary condensation takes place.[17b,19] Pt/Ketjen Black sorbs noticeably more water than Pt/Vulcan XC-72 in the range of RH between 30 and 90%, presumably because of a larger fraction of mesopores in which capillary condensation occurs, as has been reported in our earlier work.[6] It has been previously reported by Pierce et al that the presence of mesopores results in steeper water adsorption isotherms in the intermediate range of RH.[19] The point of inflection is a function of the size of the mesopores: the smaller the pore size, the lower the relative pressure at which the rise begins. The Pt/Ketjen Black adsorption curve diverges from the Pt/Vulcan XC-72 adsorption curve at 30% RH, which is attributed to the higher mesoporous volume of Pt/Ketjen Black and capillary condensation. The corresponding volumes of mesopores for Pt/Ketjen Black and Pt/Vulcan are 0.68 and 0.34 cm$^3/g_{(carbon)}$, respectively.[6]

A larger hysteresis in the intermediate range of RH in the case of Pt/Ketjen Black is attributed to the presence of an extensive pore network, i.e., trapping of larger pores in the network of smaller pores.[17b] This effect is a function of pore size distribution (PSD) of Pt/carbon. Pt/Ketjen Black was reported to possess a broader PSD with a larger fraction of low range mesopores (<20 nm), whereas Vulcan XC-72 possesses a narrower PSD, with pores mainly in the 20−100 nm range.[6]

Effect of Carbon Support and Ionomer Content. The effect of the carbon support on the overall water vapor sorption of CLs is demonstrated below. Sorption isotherms of Pt/Ketjen Black and Pt/Vulcan XC-72−based CLs with a range of ionomer loadings normalized to mass of carbon are shown in Figure 2. Corresponding Pt/carbon sorption isotherms are shown for reference. As may be seen from the figure, microstructural characteristic features of the isotherms of the native carbon supports, such as the shape of the adsorption branch of the isotherm and the hysteresis, are preserved upon addition of the ionomer. However, incorporation of ionomer results in a higher total water uptake in a CL, which increases with increasing ionomer loading.

Upon addition of the ionomer, enhanced water sorption is seen in the RH range as low as 10−30%. This might be attributed to the increase in the number of sulfonic groups of Nafion ionomer which serve as initial adsorption sites for water molecules, i.e., formation of water clusters at low RH. This effect is more pronounced with increasing ionomer loading as the number of $-SO_3^-$ groups increases.

The slightly higher total water uptakes for Pt/Ketjen Black-based CLs for identical ionomer contents are in agreement with the higher pore volume of Ketjen Black as determined by N_2-adsorption.[6] Moreover, Ketjen Black-based CLs were found to form slightly thicker CLs for identical Pt, ionomer and carbon loadings, as shown in Table 1, and thus found to be less dense and possessing larger void space where water can be incorporated.

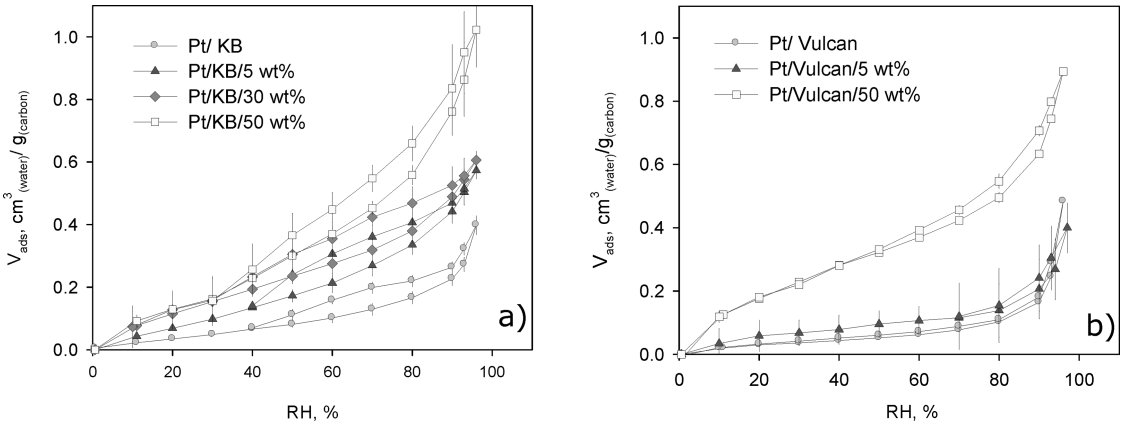

Figure 2. Water vapor sorption isotherms of (a) Pt/Ketjen CLs with 5, 30, and 50% ionomer and (b) Pt/Vulcan XC-72 with 5 and 50% ionomer normalized to carbon content.

Table 1. CL Specifications and Water Sorption Data[a]

carbon type	ionomer loading, wt %	Pt loading, mg/cm^2	carbon loading, mg/cm^2	ionomer loading, mg/cm^2	$V_{ionomer}$, cm^3/ g$_{(carbon)}$	V fraction ionomer, vol%	CL thickness, μm	V_{ads}, 20% RH, cm$^3_{H2O}$/ g$_{(carbon)}$	V_{ads}, 97% RH, cm$^3_{H2O}$/ g$_{(carbon)}$	V_{pore}, cm^3/ g$_{(carbon)}$
Ketjen Black	5	0.45	0.53	0.04	0.05	1.6	15.3 ± 2.5	0.07 ± 0.002	0.57 ± 0.03	0.86
	30	0.49	0.58	0.46	0.41	13	18.5 ± 4.0	0.11 ± 0.004	0.61 ± 0.03	0.86
	50	0.38	0.45	0.69	0.96	46	9.6 ± 0.8	0.13 ± 0.01	1.02 ± 0.20	0.86
Vulcan	5	0.40	0.48	0.05	0.05	2.5	10.0 ± 0.5	0.06 ± 0.05	0.4 ± 0.08	0.39
	50	0.32	0.38	0.67	0.96	57	9.0 ± 0.6	0.18 ± 0.03	0.9 ± 0.03	0.39

[a] Pt loading was determined using ICP. Carbon and ionomer loadings were calculated using Pt/carbon and ionomer/carbon weight ratios. CL thickness was determined by SEM; V_{pore} was determined from N_2 adsorption for Pt/carbon powders.[6].

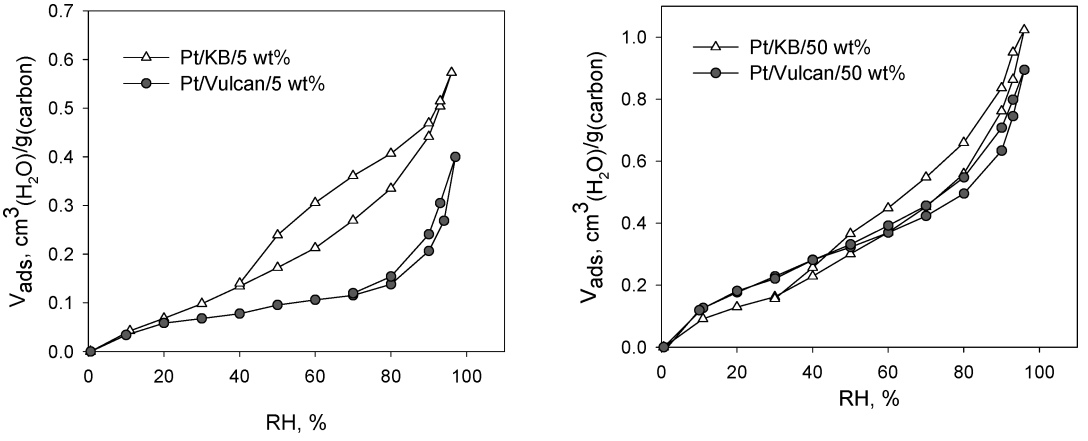

Figure 3. Water sorption isotherms normalized to mass of carbon: Pt/Ketjen (triangles) and Pt/Vulcan XC-72 (circles) CLs with 5 and 50% ionomer.

In order to compare the effect of the carbon support and ionomer content on the overall water sorption, isotherms of Ketjen Black and Vulcan XC-72-based CLs with 5 and 50 wt % ionomer in the CL are normalized to the mass of carbon in the CL as shown in Figure 3.

In the case of CLs containing 5% ionomer, Ketjen Black-based CL sorbs considerably more water than the Vulcan CL for RH > 20%. The shape of the isotherms and the hysteresis maintains the features of the corresponding carbon supports, i.e., a larger hysteresis and a higher slope of the isotherm in the intermediate RH range for the case of Ketjen Black. The higher slope of the sorption isotherm is indicative of pronounced capillary condensation in the pores of carbon and the hysteresis is indicative of enhanced water retention capacity in the pore network. In the case of CLs containing 50% ionomer, water sorption is enhanced in both carbon types. The difference in the total amount of sorbed water decreases between carbons and the microstructural characteristic features of Pt/carbon isotherms become less pronounced. This is attributed to a dominant effect of the ionomer in the water vapor sorption process at such high

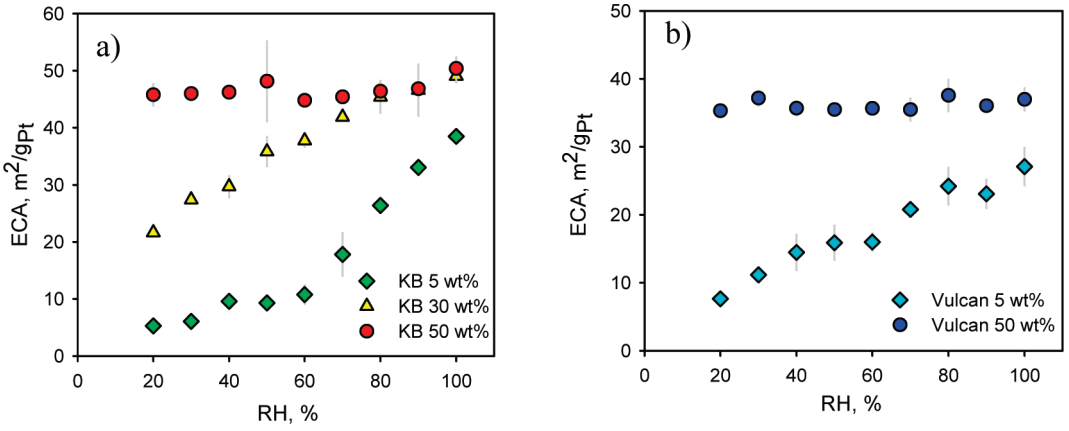

Figure 4. Electrochemical surface active area determined by cyclic voltammetry as a function of RH and ionomer content for (a) Ketjen Black CLs with 5, 30, and 50 wt % ionomer, (b) Vulcan-based CLs with 5 and 50 wt % ionomer.

ionomer contents. The effect of the carbon support microstructure on water sorption is screened at high ionomer loadings.

Electrochemically Active Surface Area. The electrochemically active surface area (ESA) attributed to the interfacial area of Pt and proton conducting phase was investigated as a function of ionomer content in the CL and as a function of relative humidity (RH). In Figure 4, it is shown that the ESA strongly depends on ionomer content as well as on RH.

Under dry conditions (20% RH), the ESA is shown to increase with ionomer loading in both CL types due to the increase in the interfacial area between Pt and the ionomer. CLs with 5 and 30 wt % ionomer also show a dramatic rise in the ESA with increasing RH from 20 to 100% RH. This increase is attributed to the growing electrochemically active interface between Pt and water as water content in the CL increases. An exponential rise in the case of 5 wt % Ketjen Black CL is attributed to the capillary condensation of water into the primary pores inside agglomerates (<20 nm), which are abundant in Ketjen Black as has been shown in our previous work.[6] Such a rapid increase in the ESA upon capillary condensation suggests that a large fraction of Pt particles is located in these pores and becomes electrochemically active only after the pores are filled with water. In contrast, a linear rise in the ESA in the case of the Vulcan 5 wt % ionomer CL suggests that Pt particles are located in the mesopores, which are easily accessible to water. Pt utilization under low RH conditions is estimated assuming the value of the ESA in 100% RH to be the total available ESA area of the CL. Then, only ~10% of available Pt is active under 20% RH in the case of Ketjen Black 5 wt % ionomer CL, in contrast to ~40% in the case of Vulcan 5 wt % ionomer CL. Interestingly, the ESA of 5 wt % ionomer CLs approaches the value of 50 wt % CLs in 100% RH, indicating that a relatively high Pt utilization can be achieved even with very low ionomer contents under fully humidified fuel cell operating conditions. By extrapolation, in the operating fuel cell, where liquid water is produced at the cathode in addition to the water supplied with the reactant gas stream, even higher ESA values might be reached. In contrast to the low ionomer content CLs, ESAs with 50 wt % ionomer seem to be RH-independent. This might be due to the relatively large amount of water initially present in the 50 wt % ionomer CL under 20% RH (~0.1 $cm^3/g_{(carbon)}$) compared to the 5 wt % ionomer CL (~0.01 $cm^3/g_{(carbon)}$) or due to prevailing sorption of water in the ionomer layer.

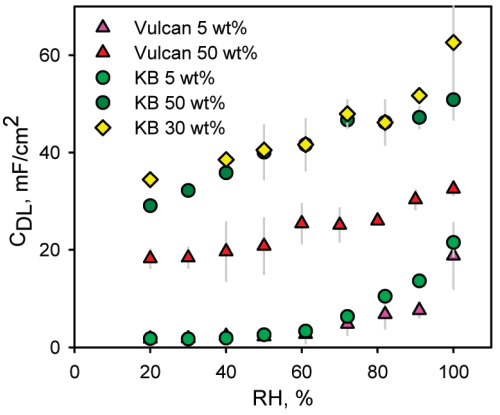

Figure 5. Double-layer capacitance of Ketjen Black and Vulcan CLs with 5 and 50 wt % ionomer as a function of RH. Ketjen Black 30 wt % CL is shown for comparison.

In addition to promoting electrochemical activity of Pt, the ionomer serves as a proton conductor to and from reaction sites. A contiguous distribution of ionomer in the CL is crucial for creating a H^+-conducting network. The ionomer distribution is correlated to the double layer capacitance (C_{DL}) of the CL, which represents Pt-ionomer and carbon-ionomer interfaces. In Figure 5, C_{DL} is plotted as a function of the ionomer content and RH. C_{DL} is found to rise with the ionomer content because of the increase in Pt−ionomer and carbon−ionomer interfacial areas. As in the case of the ESA, C_{DL} is also found to increase with RH because of contributions of Pt−water and carbon−water interfaces. In 5 wt % CLs, an insignificant variation in C_{DL} is observed in the RH range <60%, but it increases exponentially above this value. An exponential increase of C_{DL} under higher RH coincides with the onset of the capillary condensation of water in the primary pores within agglomerates (i.e., 2−20 nm size), as also observed in the plot of the ESA vs RH. A similar behavior was observed by Iden et al in a Ketjen Black−ionomer pseudocatalyst layer.[20] C_{DL} of Vulcan-based 50 wt % ionomer is lower than in Ketjen black-based 50 wt % ionomer CL, due to presumably lower total surface area of Pt/carbon available for ionomer distribution: 132 $m^2/g_{(carbon)}$ for Pt/Vulcan and 294 $m^2/g_{(carbon)}$ for Pt/Ketjen Black.[6]

The extent of Pt and carbon surface coverage by ionomer is expressed as ionomer coverage and estimated using following

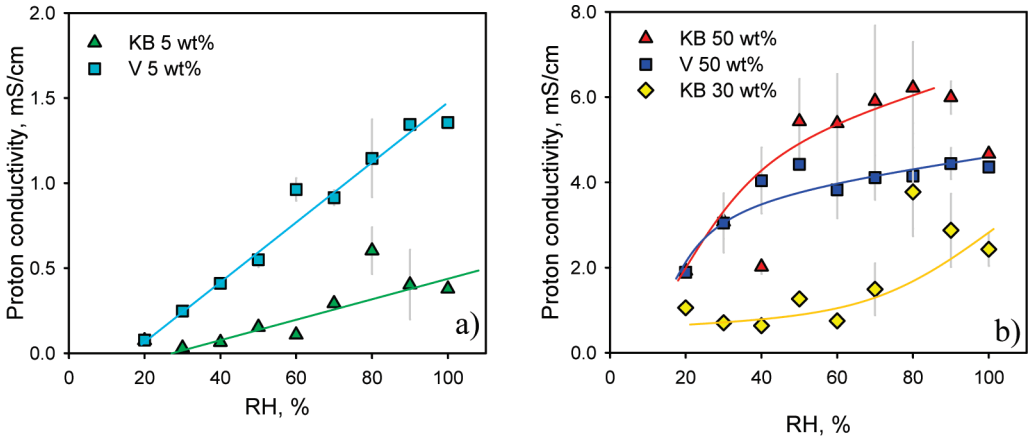

Figure 6. Proton conductivity of CLs with (a) 5 wt % ionomer loading and (b) 50 wt % ionomer loading as a function of RH. Proton conductivity of the standard 30 wt % ionomer Ketjen Black CL is shown for reference.

equation:[20]

$$\theta = \frac{C_{DL(20\%)}}{C_{DL(100\%)}} 100\% \quad (3)$$

The ionomer coverage in the Ketjen Black 5 wt % ionomer CL is estimated to be 3.5%, whereas in Vulcan 5 wt % ionomer it is 9.3%. In Ketjen Black 50 wt % ionomer it is found to be 57% coverage, and in Vulcan 50 wt % ionomer it is 56% coverage. Interestingly, in the standard Ketjen Black 30 wt % ionomer, 55% ionomer coverage is found. The similar values of the ionomer coverage in 30 and 50 wt % ionomer CLs might be attributed to the maximum ionomer coverage that is attained with 30 wt % ionomer loading, whereas further addition of ionomer results simply in an increase of the ionomer layer thickness rather than an increase in the Pt/carbon covered.

Proton Conductivity. Proton conductivity was estimated from proton resistance, R_p, in the CL and from the thickness of the CLs, determined from SEM. As seen from Figure 6, proton conductivity increases with ionomer content from 0.38−1.36 mS/cm for 5 wt % ionomer CLs to 4.04−5.18 mS/cm for 30 and 50 wt % ionomer CLs under 100% RH. This is attributed to the formation of a more connected H^+-conducting ionomer network in the CLs as the ionomer content increases. Improvement of proton conductivity in CLs is also observed with increasing RH since water serves as a proton-conducting medium alongside ionomer. Interestingly, Vulcan 5 wt % ionomer CL shows enhanced proton conductivity with increasing RH compared to the Ketjen black 5 wt % CL: 1.36 vs 0.38 mS/cm under 100% RH, respectively. This is somewhat counterintuitive since the Ketjen Black CL sorbs more water than the Vulcan CL: 0.57 vs 0.4 $cm^3_{H2O}/g_{(carbon)}$ under ∼100% RH (Table 1), and thus is expected to show an enhanced H^+-conductivity. A higher proton conductivity of Vulcan CL is attributed to its lower mesoporous surface area for ionomer distribution, which results in a more connected proton-conducting network for similar ionomer loadings.

With increasing RH, the water content in the CL increases and adsorbed water enhances proton conductivity by providing linkages between disconnected patches of ionomer in case of the 5 wt % ionomer CLs. This is expressed as a ratio of the volume of ionomer + water to the mesoporous surface area of the corresponding Pt/carbon, $V_{(I+H2O)}/SA_{(meso)}$. This ratio is found to be 34 for the Vulcan 5 wt % ionomer CL and 21 for the Ketjen Black 5 wt % ionomer CL under 100% RH, which is in agreement with observed enhanced proton conductivity of Vulcan 5 wt % ionomer CL.

Proton conductivity of both 30 and 50 wt % ionomer CLs also increases with relative humidity from ∼2 mS/cm under 20% RH to ∼5 mS/cm under 100% RH, and is mainly attributed to the increasing conductivity of hydrated ionomer layer. The values for proton conductivity of CLs reported here are in good agreement with literature data. Proton conductivity estimated by Havranek[12] for 12 vol % ionomer Vulcan-based CL is 2.6 mS/cm, which is comparable to 4.0 mS/cm for the Ketjen Black 30 wt % (i.e., 13 vol %) ionomer CL.[12] The values reported by Boyer et al[21] are somewhat higher, in the range of 10−20 mS/cm for 15 vol% ionomer CLs. The discrepancies in proton conductivity values can be attributed to differences in the CL preparation procedures as well as to variations in proton resistance measurements and data extraction methodologies.

The intrinsic proton conductivity of the ionomer in the CL is estimated by normalizing the proton conductivity of the CL to the volume fraction of ionomer in the CL. The volume fraction of ionomer is calculated from the known ionomer loading, density of ionomer, and the thickness of the CL. The values of proton conductivity of the CL and the intrinsic ionomer conductivity are compared in Table 2.

The ionomer conductivity in the CL is significantly lower than that of the bulk Nafion membrane, i.e., ∼100 mS/cm (100% RH, 80 °C) with only the Vulcan 5 wt % ionomer case approaching the Nafion bulk conductivity value. The difference could be attributed to (1) disconnectivity of the ionomer chains within the CL, which leads to the disruption of proton conducting path, (2) the lower water uptake capacity of the ionomer layer in the CL, which might be too thin for the phase-separation and formation of water-filled proton conducting channels within the ionomer layer.

Polarization Performance of Ketjen Black and Vulcan-Based CLs with 5 wt % Ionomer Content. Representative O_2 polarization curves of Ketjen Black and Vulcan based CLs containing 5 wt % ionomer under 100 and 20% RH are shown in Figure 7. The decrease in ionomer loading from 30 to 5 wt % results in a significant drop in performance under 100% RH in current density region <0.1 A/cm^2, as shown in Figure 7a. This is attributed to the lower ESAs of these CLs compared to the standard Ketjen Black 30 wt % ionomer: i.e., 27 and 39 m^2/g_{Pt} for

Table 2. Electrochemical Characteristics of Ketjen Black and Vulcan-Based CLs under 20 and 100% RH

			100% RH				20% RH			
carbon type	ionomer loading (wt %)	V_{pore} > 2 nm ($cm^3/g_{(carbon)}$)	σ_{H+} (mS/cm)	$\sigma_{H+/Vionomer\ CL}$ (mS/cm)	ESA (m^2/g_{Pt})	$V_{(H2O+I)}/SA_{(C)} \times 10^{-4}$ (cm^3/m^2)	σ_{H+} (mS/cm)	$\sigma_{H+/Vionomer\ CL}$ (mS/cm)	ESA (m^2/g_{Pt})	$V_{(H2O+I)}/SA_{(C)} \times 10^{-4}$ (cm^3/m^2)
Ketjen Black	5	0.59 ± 0.12	0.38 ± 0.02	23	38.5 ± 0.77	21	0.07 ± 0.02	4.5	5.3 ± 0.3	4.1
	30	0.35 ± 0.01	4.04 ± 0.65	31	49.1 ± 1.14	35	1.75 ± 0.65	13.5	21.6 ± 0.72	18
	50	0.08 ± 0.01	5.18 ± 0.03	17	50.4 ± 2.0	67	2.14 ± 0.04	7	45.8 ± 1.89	37
Vulcan	5	0.33 ± 0.05	1.36 ± 0.30	82	27.1 ± 2.78	34	0.08 ± 0.002	4.7	7.6 ± 0.4	8.5
	50	0.02 ± 0.001	4.4 ± 0.04	14	37.0 ± 1.6	140	1.9 ± 0.12	3.7	35.3 ± 0.21	86

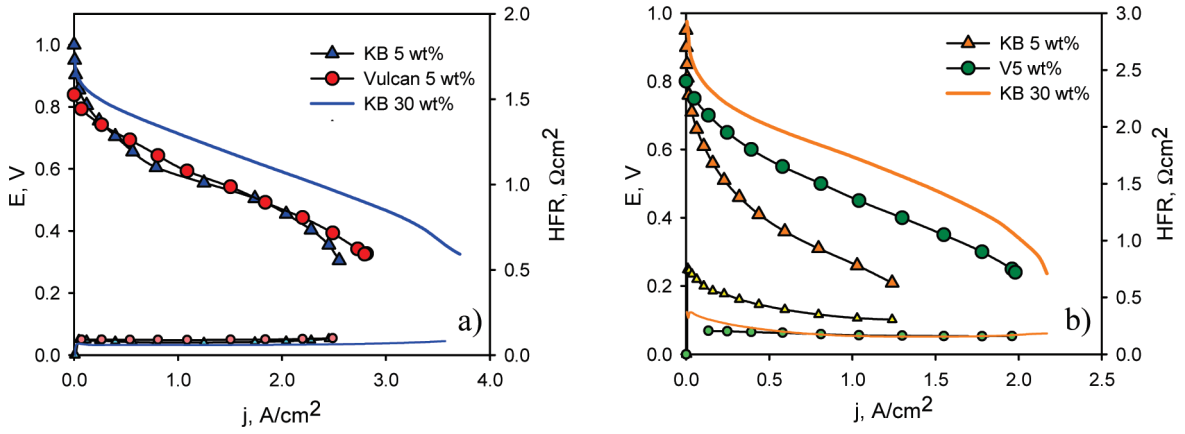

Figure 7. Polarization curves for Ketjen Black and Vulcan-based 5 wt % ionomer loading CLs (anode and cathode) under (a) 100% RH, (b) 20% RH, H_2/O_2, 2:3 stoich, atm, 80 °C, non-IR-corrected. The standard Ketjen Black 30 wt % ionomer CL is shown for reference.

Vulcan and Ketjen Black 5 wt % ionomer CLs, respectively, vs 49 m^2/g_{Pt} for the standard Ketjen Black 30 wt % CL under 100% RH, as shown in Table 2. Moreover, a sufficiently connected H^+-conducting network is necessary for protons to reach Pt particles in order for ORR to occur, however, that for ionomer loading of 5 wt % lies significantly below the percolation threshold (~30 wt %) leading to impediment of proton transport, and presumably lower proton concentration at the reaction sites. This is reflected in the low proton conductivity values: 0.38 and 1.4 mS/cm for Ketjen Black and Vulcan 5 wt % ionomer CLs, respectively, as shown in Table 2. In the high current density region, >2 A/cm^2, under fully humidified operating conditions, negligible mass transport losses are observed, especially in the case of Vulcan 5 wt % ionomer CL. This is attributed to a large pore volume available for gas transport in the CLs with 5 wt % ionomer, which is 0.59 and 0.33 $cm^3/g_{(carbon)}$ for Ketjen Black and Vulcan CLs, respectively.[6] A slightly enhanced performance of Vulcan 5 wt % CL with initially lower pore volume might be attributed to the lower water retention properties of Pt/Vulcan, as shown in Figure 3, which in turn are due to the lower fraction of pores <20 nm as discussed above. The absence of such pores in Pt/Vulcan facilitates removal of water produced on the cathode hence providing O_2 access to the reaction sites.

However, given such a low ionomer loading, the performance of these CLs is surprisingly high under 100% RH. This is attributed to the abundance of water in the CL under the fully humidified condition that functions as a proton-conducting medium and increases the ESA, as shown in Table 2.

Under dry operating conditions, water that benefits proton conduction and the ESA evaporates from the CL, and a much more significant drop in performance is observed, as shown in Figure 7b. Moreover, a clear difference in performance between two CLs is seen with the Ketjen Black 5 wt % ionomer CL experiencing a more significant performance loss in the low current density region (<0.1 A/cm^2) with respect to Vulcan 5 wt % ionomer CL. This loss in performance under given operating conditions is attributed to two factors: a more severe loss of ESA and disruption of H^+-conducting network in the Ketjen Black CL, as illustrated below. As the volume of water in the Ketjen Black 5 wt % ionomer CL decreases from 0.57 (100% RH) to 0.07 $cm^3/g_{(carbon)}$ (20% RH), the ESA drops from 38.5 to 5.3 m^2/g_{Pt}, as shown in Table 2. In the case of the Vulcan 5 wt % ionomer CL, the volume of water decreases from 0.4 (100% RH) to 0.06 $cm^3/g_{(carbon)}$ (20% RH) causing a reduction of the ESA from 27.1 to 7.6 m^2/g_{Pt}. This represents a loss of ESA of 86% and 72% in Ketjen Black and Vulcan CLs, respectively. Simultaneously, a disruption of the ionomer-water H^+-conducting network occurs. The connectivity of the proton conducting phase expressed as a ratio of volume of ionomer and water to mesoporous surface area of the carbon support, $V_{(I+H2O)}/SA_{(meso)}$, decreases under low RH. Since the ionomer contents in both 5 wt % CLs are identical and water contents are nearly the same under 20% RH (Table 1 and Figure 3), the volume of the proton conducting phase (i.e., ionomer and water) is similar in both CLs. However, the mesoporous area of Ketjen Black over which the proton conducting phase is distributed is significantly higher than

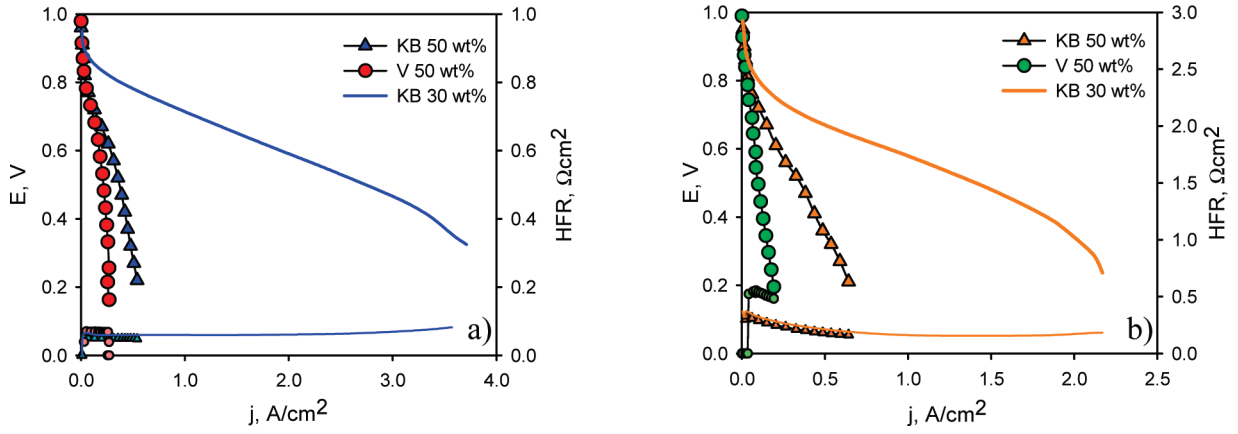

Figure 8. Polarization curves for Ketjen Black and Vulcan-based 50 wt % ionomer loading CLs (anode and cathode) under (a) 100% RH and (b) 20% RH. H_2/O_2, 2:3 stoich, atm, 80 °C, non-IR-corrected. The standard Ketjen Black 30 wt % ionomer CL is shown for reference.

that of Vulcan XC-72 (294 vs 132 $m^2/g_{(carbon)}$).[6] This may lead to a more "disconnected" ionomer network in the case of the Ketjen Black CL compared to the Vulcan CL under dry operating conditions, which is supported by the corresponding $V_{(I+H2O)}/SA_{(meso)}$ ratios of 8.5 and 4.1 for the Vulcan and Ketjen Black 5 wt % ionomer CLs, respectively. For reference, both of these $V_{(I+H2O)}/SA_{(meso)}$ values are much lower than in the standard Ketjen Black 30 wt % ionomer CL, i.e., 18, correlating well to polarization performance of these CLs. A good correlation is observed between the $V_{(I+H2O)}/SA_{(meso)}$ ratios and the ionomer coverage estimated from the double layer capacitance. The percentage of Pt/carbon surface covered by ionomer in 5 wt % ionomer CLs is 9.3 and 3.5% for the Vulcan and Ketjen Black-based CL, respectively.

From the $V_{(I+H2O)}/SA_{(meso)}$ ratios, the thickness of ionomer layer in the CL is estimated. Assuming a homogeneous distribution of the ionomer on Pt/carbon surface, ionomer layer thickness is calculated to be 0.18 nm for KB 5 wt % ionomer CL and 0.4 nm for Vulcan 5 wt % ionomer CL (294 and 132 $m^2/g_{(carbon)}$ for Ketjen Black and Vulcan, respectively), which is lower than dimensions of Nafion ionomer chains, ~ 1.2 nm diameter, used in the theoretical work of Malek et al.[22] Hence, in 5 wt % ionomer CLs, disconnected patches of ionomer are likely to be formed on the mesoporous surface of Pt/carbon. For the standard Ketjen Black 30 wt % ionomer, under the assumption of a homogeneous distribution of ionomer, the ionomer thickness is estimated to be much larger at 1.4 nm, but still unrealistically thin. Thus, based on these findings and on reported inhomogenous interactions of ionomer chains with carbon and Pt surfaces,[14] it is assumed that even in the KB 30 wt % ionomer CL the ionomer network is distributed inhomogeneously.

Polarization Performance of Ketjen Black and Vulcan-Based CLs with 50 wt % Ionomer Content. An excess of ionomer in the CL leads to impediment of gas and product water transport because of blockage of the porous space in the CL.[5c] Although it can be argued that 50 wt % ionomer CLs are of little practical significance, they are useful for fundamental understanding of the effects of ionomer and carbon in the CL on performance of the fuel cell. O_2 polarization curves of Ketjen Black and Vulcan CLs with 50 wt % ionomer loading in 100% RH are shown in Figure 8. The increase in ionomer loading from 30 to 50 wt % results in a tremendous loss in performance due to severe gas transport limitations that manifest even at very low current densities (<0.1 A/cm^2). Despite the adequate ESA and proton conductivity in these CLs (50.4 m^2/g_{Pt} and 5.2 mS/cm for Ketjen Black 50 wt % ionomer CL; and 37.0 m^2/g_{Pt} and 4.4 mS/cm Vulcan 50 wt % ionomer CLs), as listed in Table 2, high ionomer and water contents hinder the reactant gases from reaching the active sites though the ionomer and water filled pores. Pore volume is negligibly small in both CLs: 0.08 and 0.02 $cm^3/g_{(carbon)}$ for Ketjen Black and Vulcan-based CLs, respectively.[6] The thickness of ionomer and water layer is estimated to be ~14 and 7 nm thick. Such a thick layer of ionomer/water layer is expected to block the majority of the pores.

Under dry operating conditions, where little water is present in the CLs, the performance deteriorates further, as shown in Figure 8b. Despite the relatively high values of the ESA (46 and 35 m^2/gPt for Ketjen Black and Vulcan CLs, respectively) and adequate proton conductivity (2.1 and 1.9 mS/cm for Ketjen Black and Vulcan CLs, respectively), dramatic losses are observed at current densities <0.1 A/cm^2, as shown in Table 2. Although evaporation of water provides more available pore space for gas transport, oxygen penetration through a dry ionomer layer decreases significantly. Oxygen permeability through a dry Nafion film is an order of magnitude smaller than through a hydrated film: 2.84×10^{-15} mol/s/m/Pa in dry Nafion vs 2.62×10^{-14} mol/s/m/Pa in hydrated Nafion, as estimated from data provided by Sakai et al.[23] Thus, performance losses in 50 wt % ionomer CLs are attributed mainly to oxygen transport limitations to the reaction sites due to decrease of pore space for gas transport and lower permeability of O_2 through the dry ionomer layer.

In Figure 9, a schematic of Ketjen Black and Vulcan XC-72-based CLs with 5, 30, and 50 wt % ionomer loading are shown upon water sorption. In 5 wt % ionomer CLs, water is shown to provide linkages between disconnected patches of ionomer; ionomer and water contents are however low enough to leave unoccupied pore space and provide a direct gas access to the reaction sites, i.e., active reaction sites. As the ionomer content increases, pore space becomes filled with ionomer and water to the larger extent in the case of Vulcan-based CLs because of its initially lower pore volume, and the active sites become blocked to gas access.

Asymmetrical MEAs with Lowered Ionomer Content. Summarizing the findings presented above, a high ionomer loading in the CL (≥30 wt %) and a carbon support with a

broad PSD, such as the Ketjen Black type, should facilitate sorption and retention of water in the CL, and thus are assumed to be beneficial for the anode CL, which is prone to dehydration due to the electroosmotic drag. On the other hand, a lower ionomer loading (<30 wt %) and a carbon support with a narrower PSD in the mesoporous range, i.e., Vulcan type, should facilitate water removal and hence is expected to be beneficial for the cathode CL. Based on these considerations, fuel cell performance of MEAs comprising of an anode and a cathode of different compositions, i.e., type of carbon and ionomer loading, were evaluated. An asymmetrical MEA with a hydrophilic anode (Ketjen Black 30 wt % ionomer CL (KB30)) and a hydrophobic cathode (Vulcan 5 wt % ionomer CL (V5)) was used to assess the fuel cell performance. A "mirror image" MEA with a hydrophobic anode and a hydrophilic cathode (V5KB30) was examined to verify the presented hypothesis. Fuel cell performance curves of KB30V5 and V5KB30 MEAs under oxygen and air in 100% RH are shown in Figure 10.

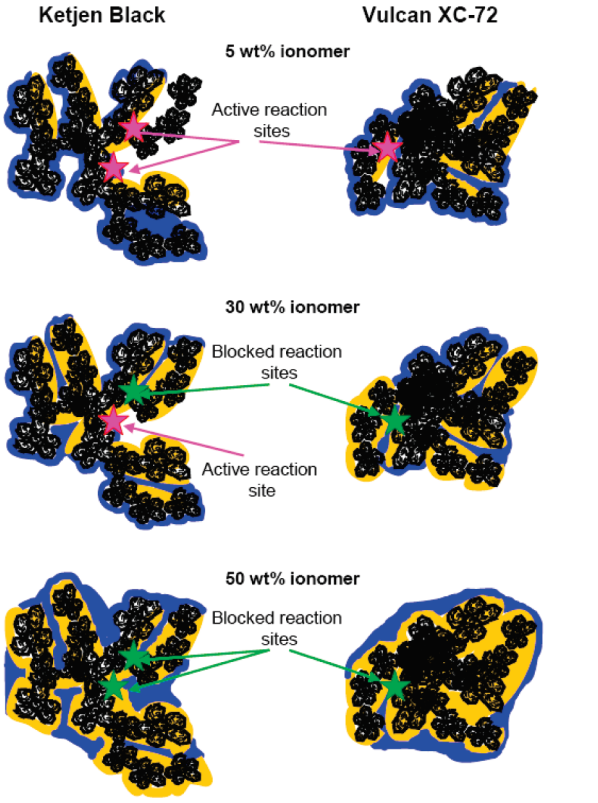

Figure 9. Schematic illustrating ionomer and water distribution in the mesopores of Pt/carbon with 5, 30, and 50 wt % ionomer. The active reaction sites that are in contact with gas, proton and electron conducting phases are shown in pink. The reaction sites with a hindered gas access by ionomer and water, i.e., blocked sites, are shown in green.

It is seen that both asymmetrical MEAs perform very similar to the standard Ketjen Black 30 wt % ionomer MEA despite a significantly lower ionomer loading of one of the electrodes. As predicted, KB30V5 shows an enhancement in the mass transport region, especially, under operation in air. However, a large loss in the kinetic and Ohmic region, similar to that seen in the symmetrical 5 wt % ionomer MEAs, is observed. This loss is attributed to the low ESA (27.1 vs 49.1 m^2/g_{Pt} for V5 and KB30 electrodes, respectively) and a lower proton conductivity (1.36 vs 4.04 mS/cm for V5 and KB30 electrodes, respectively) of the Vulcan 5 wt % ionomer cathode.

On the other hand, V5KB30 MEA performs nearly identically to the standard KB30KB30 in the low current density region but diverges at the current density of ~1A/cm^2. It is interesting to note that reduction of the ionomer loading on the anode from 30 wt % to 5 wt % ionomer does not seem to have a detrimental effect on the performance of the MEA up to current density of 1 A/cm^2, thus suggesting that the kinetic region is controlled by the ORR reaction on the cathode. However, in the high current density region (1−3.5 A/cm^2) a notable performance loss is observed, which is attributed to the dehydration of the anode because of the electroosmotic drag and subsequent disruption of proton-conducting network at very high current densities under operation in oxygen, and because of flooding of the cathode under operation in air.

Under dry operating conditions (20% RH), reduced water content in the CL has a significant impact on the performance of MEAs as shown in Figure 11. KB30V5 MEA suffers a drastic loss in the kinetic region at the current densities <0.1 A/cm^2. This is attributed to the decrease in the ESA from 27.1 to 7.6 m^2/g_{Pt} and a decrease of proton conductivity from 1.36 to 0.08 mS/cm on the V5 cathode under low RH conditions, refer to Table 2. The performance of the V5KB30 MEA is significantly higher under dry operating conditions and is nearly identical to the

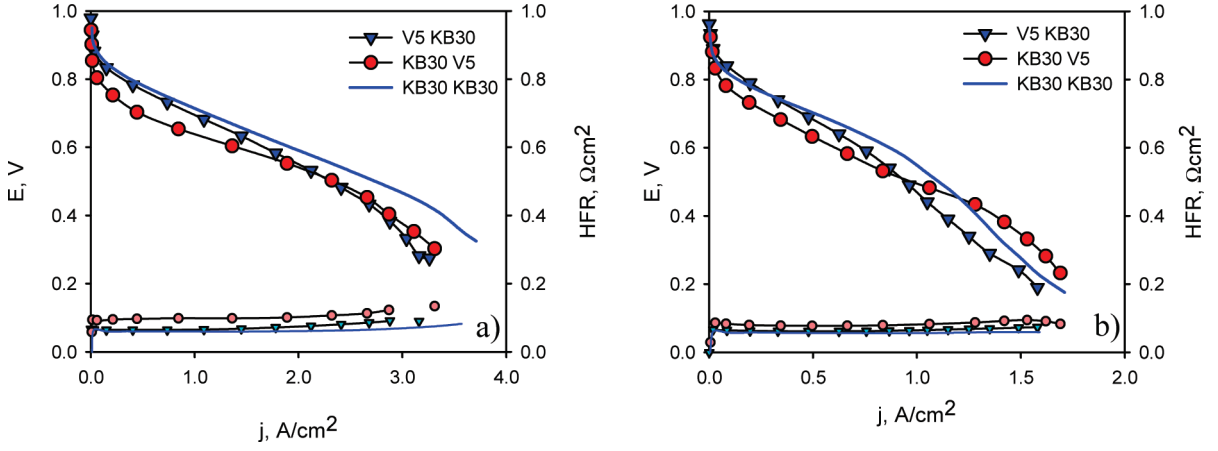

Figure 10. (a) Oxygen and (b) air polarization curves for KB30 V5 and V5KB30 MEAs in 100%RH, 2:3 stoich, atm, 80 °C, non-IR-corrected. The standard Ketjen Black 30 wt % ionomer CL is shown for reference.

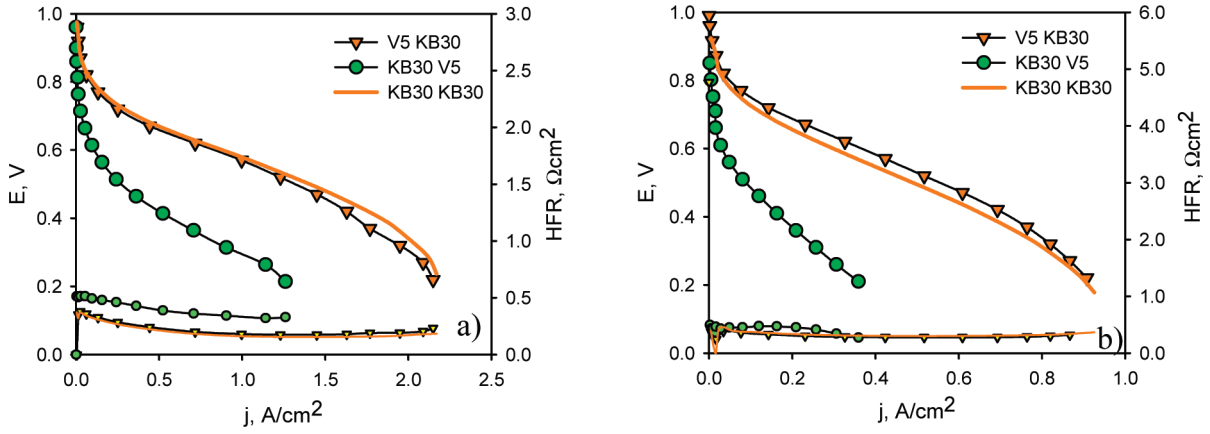

Figure 11. (a) Oxygen and (b) air polarization curves for KB30 V5 and V5KB30 MEAs under 20% RH, 2:3 stoich, atm, 80 °C, non-IR-corrected. The standard Ketjen Black 30 wt % ionomer CL is shown for reference.

performance of the standard KB30KB30 MEA. This is attributed to a relatively high ESA of 21.6 m^2/g_{Pt} and a proton conductivity of 1.75 mS/cm under 20% RH in the KB 30 wt % ionomer cathode. Interestingly, under this operating condition, a much lower ionomer content Vulcan 5 wt % ionomer anode does not have a negative impact on CL performance compared to the standard Ketjen Black 30 wt % anode in the standard 30 wt % ionomer MEA.

Based on the polarization curves of the asymmetrical MEAs presented above, it is speculated that the ionomer loading can be reduced in one of the CLs in an MEA without dramatic performance losses. However, whether the reduction is performed on the anode or the cathode depends on the operating conditions of the fuel cell. If the operation under low RH is required, as often requested by automotive applications,[24] a reduction of the anode ionomer loading from 30 to 5 wt % ionomer can be achieved without notable performance losses. A reduction of the ionomer loading on the cathode might be meaningful in order to improve performance in the mass transport region if the fuel cell is operated under fully humidified conditions in the air environment.

CONCLUSIONS

The microstructure of conventional catalyst layers has a significant impact on water sorption and retention properties of CLs and on fuel cell performance. Water sorption properties depend on the pore size distribution of the employed carbon and ionomer loading in the CL. The larger the fraction of mesopores (<20 nm), the more pronounced the capillary condensation of water in these pores and, thus, the water uptake in the CL. The broad PSD with a large fraction of pores <20 nm, as in Ketjen Black, results in higher degree of water retention in the CL. Incorporation of ionomer into the CL is found to enhance its water sorption.

It was found that in the CLs with a low ionomer loading of 5 wt %, adequate utilization of Pt can be achieved under high RH condition because of electrochemical activity of water in the catalyst layer. Water sorbed in the CL compensates for low ionomer content in terms of ESA and proton conductivity, and the carbon microstructure does not have a notable effect, but it does become crucial under low RH condition. Because of the structural nature of Ketjen Black, i.e., large fraction of pores <20 nm, where Pt particles seem to be located, much Pt remains inactive until water condenses in these pores in the high RH range. Thus, the location of Pt in intra-agglomerate mesopores <20 nm might be considered disadvantageous for the fuel cell operation under low RH condition.

An optimum value of ionomer content in the catalyst layer is a function of surface area of pores >20 nm — the higher the mesoporous surface area, the higher ionomer content is required to create a continuous proton conducting network (assuming an even ionomer distribution on mesoporous surface). The lower surface area of Vulcan is shown to be beneficial for creating a more connected H^+-conducting network in 5 wt % ionomer CL, which is due to the proportionally higher ionomer coverage. The $V_{(I+H2O)}/SA_{(meso)}$ ratio is a useful parameter for estimating the connectivity of the water + ionomer network and could be employed for evaluating the optimal ionomer loading for a particular carbon.

On the basis of these findings, we speculate that mesoporous carbons with relatively low surface area (~200 m^2/g) and a negligible fraction of micropores (<2 nm) are beneficial for the purpose of decreasing ionomer content in the CL while maintaining adequate fuel cell performance. The lower the mesoporous area, the lower the ionomer loading that is required for formation of a connected ionomer network. Platinum, if located in the mesopores, is in the direct contact with ionomer and the gas phase over a wide range of RH as opposed to Pt located in the pores <20 nm inside agglomerates that are filled with water upon capillary condensation. Production of liquid water at the cathode during fuel cell operation is believed to have a particularly beneficial effect on proton conductivity of low ionomer cathode catalyst layers.

It is suggested that catalyst supports with a broad pore size distribution are advantageous to the anode, whereas supports with a narrower pore size distribution facilitate water removal from the cathode CLs, thus alleviating flooding. The ionomer content might be varied on the anode and the cathode depending on the mesoporous surface area of the carbon support employed and depending on fuel cell operating conditions. The hypothesis is confirmed for fuel cell operating under high relative humidity in air. However, in the low relative humidity operation, the low ionomer content on the cathode seems to be detrimental for the fuel cell performance. This is assumed to be due to decrease in the ESA and disruption of the water−ionomer H^+-conducting

network. On the other hand, a low ionomer content on the anode does not seem to have a notable negative impact on the total fuel cell performance under dry operating conditions.

AUTHOR INFORMATION

Corresponding Author
*Phone: +1 778 782 4221. Fax: +1 778 782 3765. E-mail: holdcrof@sfu.ca.

ACKNOWLEDGMENT

The authors thank NRC-IFCI, NSERC, and SFU for financial support. Tanaka Kikinzoku Kogyo and Cabot Corp. for providing carbon and catalyst materials.

REFERENCES

(1) Ticianelli, E. A.; Derouin, C. R.; Redondo, A.; Srinivasan, S. *J. Electrochem. Soc.* **1988**, *135*, 2209.
(2) (a) Wilson, M. S.; Gottesfeld, S. *J. Electrochem. Soc.* **1992**, *139*, L28. (b) Wilson, M. S.; Gottesfeld, S. *J. Appl. Electrochem.* **1992**, *22*, 1.
(3) (a) Litster, S.; McLean, G. *J. Power Sources* **2004**, *130*, 61. (b) Antolini, E. *J. Appl. Electrochem.* **2004**, *34*, 563.
(4) Fontanella, J. J.; McLin, M. G.; Wintersgill, M. C.; Calame, J. P.; Greenbaum, S. G. *Solid State Ionics* **1993**, *66*, 1.
(5) (a) Li, G. C.; Pickup, P. G. *J. Electrochem. Soc.* **2003**, *150*, C745. (b) Gode, P.; Jaouen, F.; Lindbergh, G.; Lundblad, A.; Sundholm, G. *Electrochim. Acta* **2003**, *48*, 4175. (c) Passalacqua, E.; Lufrano, F.; Squadrito, G.; Patti, A.; Giorgi, L. *Electrochim. Acta* **2001**, *46*, 799.
(6) Soboleva, T.; Zhao, X. S.; Mallek, K.; Xie, Z.; Navessin, T.; Holdcroft, S. *ACS Appl. Mater. Interfaces* **2010**, *2*, 375.
(7) (a) Eikerling, M. *J. Electrochem. Soc.* **2006**, *153*, E58. (b) Eikerling, M.; Ioselevich, A. S.; Kornyshev, A. A. *Fuel Cells* **2004**, *4*, 131−140. (c) Eikerling, M.; Kornyshev, A. A. *J. Electroanal. Chem.* **1998**, *453*, 89.
(8) Adachi, M.; Navessin, T.; Xie, Z.; Frisken, B.; Holdcroft, S. *J. Electrochem. Soc.* **2009**, *156*, B782.
(9) (a) Nam, J. H.; Kaviany, M. *Int. J. Heat Mass Transfer* **2003**, *46*, 4595. (b) Lim, C.; Wang, C. Y. *Electrochim. Acta* **2004**, *49*, 4149.
(10) (a) Li, X. G.; Sabir, I.; Park, J. *J. Power Sources* **2007**, *163*, 933. (b) Xue, D.; Dong, Z. *J. Power Sources* **1998**, *76*, 69.
(11) Cooper, K. R.; Ramani, V.; Fenton, J. M.; Kunz, R. *Experimental methods and data analysis for polymer electrolyte fuel cells*; Scribner Associates, 2005.
(12) Havranek, A.; Wippermann, K. *J. Electroanal. Chem.* **2004**, *567*, 305.
(13) Kinoshita, K., *Carbon: Electrochemical and Physicochemical Properties*; Wiley: New York, 1988.
(14) Volfkovich, Y. M.; Sosenkin, V. E.; Nikolskaya, N. F. *Russ. J. Electrochem.* **2010**, *46*, 438.
(15) (a) Sing, K. S.; Everett, D. H.; Haul, R. A.; Moscou, L.; Pierotti, R. A.; Rouquerol, J.; Siemieniewska, T. *Pure Appl. Chem.* **1985**, *57*, 603. (b) Rouquerol, J.; Avnir, D.; Fairbridge, C. W.; Everett, D. H.; Haynes, J. H.; Pernicone, N.; Ramsay, J. D.; Sing, K. S.; Unger, K. K. *Pure Appl. Chem.* **1994**, *66*, 1739.
(16) Kiselev, A. V. *2nd International Congress on Surface Activity*; Butterworths: London, 1957; p 219.
(17) (a) Muller, E. A.; Gubbins, K. E. *Carbon* **1998**, *36*, 1433. (b) Gregg, S. J.; Sing, K. S. W. *Adsorption, Surface Area and Porosity*; Academic Press: New York, 1982.
(18) (a) Kiselev, A. V.; Kovaleva, N. B.; Korolev, A. I.; Shcherbakova, K. D. *Dokl. Akad. Nauk SSSR* **1959**, *124*, 617. (b) Walker, P. L.; Janov, J. *J. Colloid Interface Sci.* **1968**, *28*, 449.
(19) Pierce, C.; Smith, R. N.; Wiley, J. W.; Cordes, H. *J. Am. Chem. Soc.* **1951**, *73*, 4551.
(20) Iden, H.; Ohma, A.; Shinohara, K. *J. Electrochem. Soc.* **2009**, *156*, B1078.
(21) Boyer, C.; Gamburzev, S.; Velev, O.; Srinivasan, S.; Appleby, A. J. *Electrochim. Acta* **1998**, *43*, 3703.
(22) Malek, K.; Eikerling, M.; Wang, Q. P.; Liu, Z. S.; Otsuka, S.; Akizuki, K.; Abe, M. *J. Chem. Phys.* **2008**, *129*, 204702.
(23) Sakai, T.; Takenaka, H.; Torikai, E. *J. Electrochem. Soc.* **1986**, *133*, 88.
(24) Costamagna, P.; Srinivasan, S. *J. Power Sources* **2001**, *102*, 242.